Recent Advances in the Long-Wavelength Radio Physics of the Sun

N. Gopalswamy NASA Goddard Space Flight Center, Greenbelt, MD 20771, USA
gopals@fugee.gsfc.nasa.gov

(Submitted to Planetary and Space Science, October 16, 2003; Revised March 31, 2004)

Abstract

Solar radio bursts at long wavelengths provide information on the solar disturbances such as coronal mass ejections and shocks at the moment of their departure from the Sun. The radio bursts also provide information on the physical properties (density, temperature and magnetic field) of the medium that supports the propagation of the disturbances with a valuable cross-check from direct imaging of the quiet outer corona. The primary objective of this paper is to review some of the past results and highlight recent recent results obtained from long-wavelength observations. In particular, the discussion will focus on radio phenomena occurring in the outer corona and beyond in relation to those observed in white light. Radio emission from nonthermal electrons confined to closed and open magnetic structures and in large-scale shock fronts will be discussed with particular emphasis on its relevance to solar eruptions. Solar cycle variation of the occurrence rate of shock-related radio bursts will be discussed in comparison with those of interplanetary shocks and solar proton events. Finally, case studies describing the newly-discovered radio signatures of interacting CMEs will be presented.

1 Introduction

The seven to eight decades of the radio window (300 GHz to 3 kHz) essentially correspond to the plasma frequencies prevailing in the solar chromosphere to the far reaches of the interplanetary medium. Radio emissions related to the plasma frequencies provide information on the physical conditions prevailing at the plasma levels. The Sun produces radio emission by thermal and nonthermal processes (see, e.g. Kundu, 1965; Zheleznyakov, 1969 for reviews). Solar plasmas have temperatures ranging from a few thousand K in the chromosphere and prominences to tens of MK in flare loops and ejecta. Thermal emission from these plasmas produces significant levels of radiation at long radio wavelengths. Nonthermal emission is caused by electrons accelerated at the Sun during transient processes such as flares and coronal mass ejections (CMEs). The intensity and spectrum of the emitted radiation depend on the emission mechanism, which in turn depends on the density, temperature, and magnetic field (strength and topology) of the source plasma as well as on the distribution of the accelerated electron population. Radio waves produced by shocks and electron beams during solar eruptions belong to the longer wavelength section of the radio window. Radio observations can track these disturbances throughout the Sun-Earth connected space, thus providing physical information on both the disturbances and the interplanetary space that supports the propagation. Interplanetary scattering of radio waves from natural and man-made radio sources and the scattered radiation provides valuable information on the turbulence spectrum of the interplanetary medium. The radio technique, perfected over half a century, continues to be a unique way of probing those regions of space where *in situ* observations can be made only in the distant future.

The long-wavelength radio phenomena occur at meter (m) to kilometric (km) wavelengths. Radio emission at meter wavelengths originates from the corona close to the Sun while the kilometric emission originates in the inner heliosphere. This ordering of longer wavelength emission originating from greater distances from the Sun is due to the decrease of plasma density away from the Sun. The electron density n decides the characteristic plasma frequency f_p by the relation, f_p (Hz) $= 9{\times}10^3\sqrt{n}$ (cm^{-3}). Electron density measurements from eclipse observations indicate that a plasma frequency of 30 MHz occurs at a heliocentric distance of $\sim$ 2 R$_\odot$. The corresponding electron density is $1.1{\times}10^7$ cm^{-3}. The density falls to $\sim$ 10^6 cm^{-3} (plasma frequency is $\sim$ 10 MHz) at a heliocentric distance of 3 R$_\odot$. Interestingly, this plasma density is comparable to the electron density in the day-time terrestrial ionosphere. Therefore, radio emission at frequencies below 10 MHz cannot penetrate the ionosphere. So we must go to space to observe radio emission originating at distances beyond a few R$_\odot$ from the Sun. Space radio instruments thus observe the interplanetary (IP) radio emission while ground based instruments can detect the coronal radio emission.

Although solar radio observations have been made for more than six decades, imaging observations were very limited. Spatially resolved observation is essential to understand most of the transient phenomena on the Sun that produce nonthermal radio emission. The Culgoora (McLean and Labrum, 1985) and Clark Lake (Kundu et al., 1983) radioheliographs, which operated in the 1970's and 1980's obtained 2-D images of the quiet Sun and the transient phenomena. Images of type I storms, type III bursts from electron beams, type II bursts from shock waves, and moving type IV bursts were obtained by the radioheliographs (see McLean and Labrum, 1985 for a review). The imaging observations also raised some interesting questions about the origin of shock waves and electron beams, which are still not fully answered. Unfortunately these observatories were closed long ago leaving a huge deficit in spatially-resolved data. The Nançay radioheliograph (Kerdraon and DeLouis, 1997) operates at frequencies less than ideal for imaging at long-wavelength radio phenomena, although it provides useful information on the early stages of solar eruptions (see, e.g., Maia et al., 2000). The only other imaging instrument is the Gauribidanur Radioheliograph (Ramesh et al. 1998), which has started producing excellent complementary information on CMEs close to the Sun (Kathiravan et al., 2002). Radio imaging of the Sun at long wavelengths has never been done from space. Space radio instruments have been designed to provide at least some information on the location of the radio source by using direction-finding techniques. For example, the analysis of the signals on orthogonal dipole antennas can provide the azimuth and latitude to the centroid of the radio source. This analysis also helps estimate the size of the radio source. One can also use three approximately orthogonal dipole antennas on a non-spinning, three-axis stabilized spacecraft to measure the cross-correlations to yield the direction and size of the radio sources. True imaging is essential for understanding the physics behind the radio emission, which depends on the spatial structure and time dependence of the source of nonthermal electrons.

In order to see the level of long-wavelength radio emission in comparison with shorter wavelength coronal emissions, we have shown in Fig. 1 the flux density of various radio phenomena from short wavelengths ($\leq$ 10 m, observed from ground) to long wavelengths ($>$ 10 m, observed from space). The flux density of radio bursts (Types II and III) is the largest at all wavelengths. The flux density in the IP medium is dominated by radio bursts. Note that the IP radio emission is less complicated compared to the coronal emissions. The IP radio phenomena can be ordered from highest to lowest flux density as follows: Type III bursts, Type II bursts, Type III storm, galactic background, and Quiet Sun emission. In this paper, we provide an outline of the radio

phenomena at long wavelengths, especially in the IP medium with a particular emphasis on the recent results obtained from the Radio and Plasma Wave (WAVES) experiment on board the Wind spacecraft (Bougeret et al., 1995). WAVES has two receivers operating in the frequency ranges 20 to 1040 kHz (RAD1) and 1.075 to 13.825 MHz (RAD2). The RAD2 spectral range (marked DH in Fig. 1 to denote the decameter-hectometric band from 21 m to 300 m) became available for the first time in 1994 and filled a crucial gap between ground and space based observations. Simultaneous white light observations of the corona obtained by the Solar and Heliospheric Observatory (SOHO) have also contributed enormously in the interpretation of the radio phenomena. Therefore, most issues discussed in this paper will draw extensively from SOHO observations.

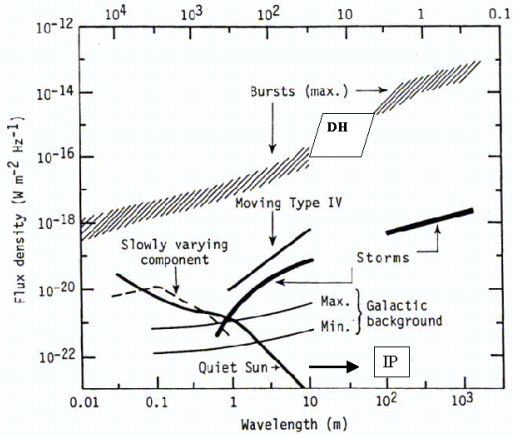

Figure 1: Schematic diagram showing the flux densities of various radio phenomena 0.01 m to $>$ 1km. In the top, the corresponding frequencies are marked in MHz. The gap between 10 and 100 m (decameter to hectometer wavelengths, or DH for short) was due to the wavelengths employed by ground based and space based radio observations. This gap was filled by the launch of Wind/WAVES experiment as indicated by the parallelogram 'DH'. Radio emission at wavelengths longer than 10 m are considered interplanetary (IP). The flux density of Types II and III radio bursts is the largest at all wavelengths, as marked by "Bursts (max.)". The maximum and minimum observed flux densities of the galactic background are also shown. The galactic background rises a bit more and peaks around 100 m with a flux density of $10^{-19} W\ m^{-2}$ Hz^{-1}. The quiet Sun emission falls below the galactic background, but the type III storms and interplanetary radio bursts of type III and type IV are much brighter than the galactic background. (Adapted from McLean and Labrum, 1985).

2 Thermal Radio Emission

Although the thermal emission from the corona peaks in soft X-rays (the temperature of the corona is $\sim$ 2 MK), there is significant radio emission at long wavelengths. Thermal emission at a given frequency mostly originates from close to the plasma level of that frequency, where

the emission becomes optically thick. The observed brightness temperature is close to the temperature at the local plasma level. Thus the radio Sun is larger at lower frequencies. Ground based interferometric imaging has shown that the radio Sun extends to a few solar radii. Even though the galactic background has a larger flux density, it is possible to image the quiet Sun because an interferometric array can resolve out large structures like the galactic background. Fig. 2 shows a set of quiet Sun images obtained by the Clark Lake Radioheliograph at four frequencies. The observations were made close to the solar minimum (1985 August 3) so the corona is dominated by the equatorial streamer belt. This fact is faithfully reflected in the elongation of the radio contours in the equatorial region. In addition to the streamer structure, a coronal hole can also be seen in the northeast quadrant. Thus the quiet Sun imaging provides important information on the large-scale structure of the corona. A combination of radio imaging and modeling can provide independent information on the electron density distribution in the corona.

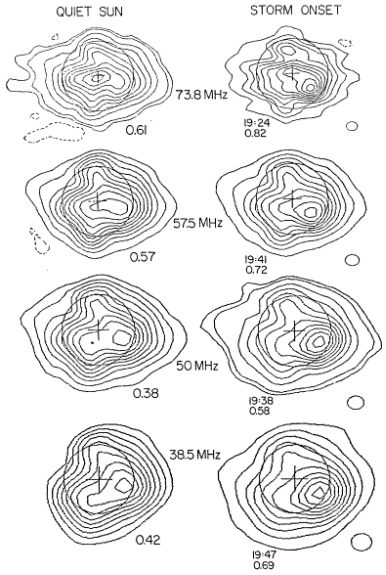

Figure 2: Contour images of the quiet Sun and the onset phase of a noise storm obtained by the Clark Lake Radioheliograph at four frequencies on 1985 August 3. The contour levels are plotted at 10% intervals of the peak brightness temperature (marked directly below the images in units of MK). The lowest and highest contour levels are at 15% and 95% of the peak brightness temperature. The Quiet Sun maps show the streamer to the west and coronal holes to the north-east. The small ellipses below the images denote the size of the beam (spatial resolution) of the imaging array (see Kundu and Gopalswamy, 1990 for more details).

The peak in the brightness temperature occurs in the southwest quadrant, where a weak nonthermal type I storm started later. Note that the radio images contain both the thermal and

nonthermal components. The dynamic range of the image decides the weakest feature that can be discerned from the images. When the nonthermal emission gets stronger, it would become difficult to see the weak thermal component.

CMEs contain coronal material at the coronal temperature (except for the core, which may or may not be hot), but the density is higher than the surroundings. The excess density is observed as enhanced thermal bremsstrahlung emission, which can be imaged at radio wavelengths. Direct imaging of coronal streamer changes (Sheridan et al., 1978) and CMEs (Gopalswamy and Kundu, 1992a) have already been demonstrated. Figure 3 shows a set of three radio contour images obtained by the Clark Lake radioheliograph. The last two images contain the CMEs, which are clearly different from the pre-CME image. By subtracting the pre-CME image from the last two, one can isolate the CME as a thermal source (see e.g., Gopalswamy and Kundu, 1992a). Since the radio emission mechanism is well understood, it is straightforward to compute the mass contained in the CME according to the formula (Gopalswamy and Kundu, 1992a), $M_{cme} = 2\times10^{-24}[5L^{-1}T_bT^{1/2}f^2]^2V$, where L is the thickness of the CME along the line of sight, T_b is the observed excess brightness temperature (the radio CME), T is the coronal temperature, f is the observing frequency, and V is the CME volume estimated from the radio images. Masses obtained from this formula are quite similar to those of white-light CMEs (Gopalswamy and Kundu, 1993; Ramesh et al., 2003). Since the radiation in white-light and radio has different physical origins (Thomson-scattering in white light and bremsstralung in radio), the radio method provides an independent technique to estimate CME masses. CME substructures such as the coronal cavity (or filament channel) are now routinely observed as changes in CME-related thermal emission by the Nançay Radioheliograph (Marqué et al., 2002).

3 Type IV Bursts

Nonthermal electrons trapped in moving or stationary structures produce long-lasting continuum emissions known as type IV bursts and have been extensively studied at metric wavelengths (see e.g., Stewart, 1985; Robinson, 1985 for reviews). Stationary type IV bursts are also known as flare continua (Robinson, 1985) because they occur in association with flares. Nonthermal electrons responsible for the flare continua are thought to be accelerated at the flare site or by a shock wave and get trapped in closed magnetic field structures. Moving type IV bursts are closely related to CMEs because, the radio emitting structures move as expanding arches or advancing fronts associated with CMEs. The heated prominence material can also trap electrons and propagate as isolated plasmoids (Gopalswamy and Kundu, 1990) imaged at radio wavelengths. Without spatially resolved observations, it is difficult to detect moving type IV bursts. The observed spectrum of moving type IV bursts is consistent with Razin-suppressed gyrosynchrotron emission from nonthermal electrons trapped in moving magnetic structures (Gopalswamy and Kundu, 1990; Bastian et al., 2001). Figure 4 gives the typical brightness temperatures ($\sim10^7$ K) of moving type IV bursts at meter-decametric wavelengths. The computed brightness temperature spectrum in the presence of ambient plasma (curves labeled as 'MEDIUM') shows a better agreement with the observations than the one without (curves labeled 'VACUUM'). The observed and computed spectra indicate that the brightness temperatures at frequencies as low as 15 MHz are still significant that the burst can be imaged at long wavelengths from ground and space.

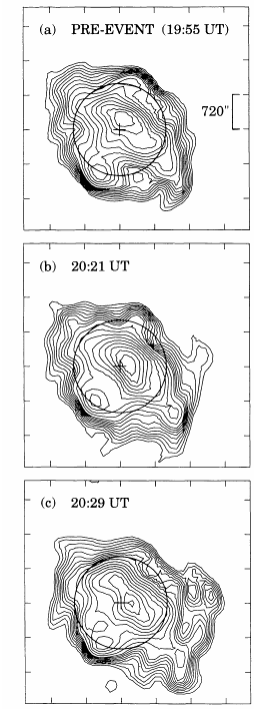

Figure 3: Contour images of the Sun on 1986 February 16 at three instances as obtained by the Clark Lake radioheliograph at 73.8 MHz. The top panel shows the pre-event radio Sun. The middle and bottom panel show the modification of the quiet Sun emission due to the appearance of a CME. The CME was observed by the Solar Maximum Mission (see Gopalswamy and Kundu, 1992a for details).

3.1 Decametric Type IV bursts

Wind/WAVES has observed only a dozen type IV events from its launch in 1994 until 2002. Comparison with meter wave observations reported by the Solar Geophysical Data revealed that most of the WAVES type IV events had metric counterparts. Therefore, the WAVES type IV bursts are just the longer-wavelength extensions of the metric type IV bursts. Figure 5 illustrates a type IV burst observed by WAVES on 2002 August 16. The onset of the type IV burst was preceded by type II and type III bursts and a fast halo CME (speed $\sim$1500 km s^{-1}). The U-shaped low-frequency edge in the dynamic spectrum is characteristic of all the WAVES type IV bursts. Figure 6 gives the statistical properties of the 12 WAVES type IV bursts detected until the end of 2002. All were associated with fast CMEs (average speed $\sim$ 1200 km s^{-1}). The CMEs were also very wide: all but three of the CMEs were halos and the rest were partial halos. The typical duration of the bursts measured at 14 MHz was $\sim$2 h. The ending frequency of the type IV bursts was never below $\sim$ 6 MHz (average is 7.7 MHz). Thus in almost all the cases

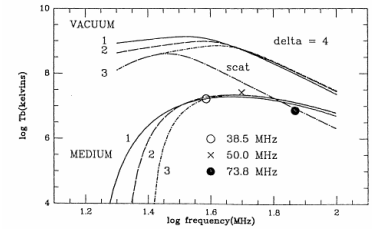

Figure 4: Observed and computed brightness temperature spectrum of a moving type IV burst imaged by the Clark Lake Radioheliograph. The observing frequencies were 73.8, 50 and 38.5 MHz and the corresponding data points are marked by open circle, cross, and filled circle, respectively. The three curves (1, 2, and 3) represent three plausible sets of parameters (nonthermal electron density and spectral index (delta), electron density and ambient plasma density and the strength of the magnetic field). The top three curves are for vacuum and the bottom three (marked MEDIUM) are with significant ambient density to cause Razin suppression. The curve denoted by "scat" is a variant of the curve VACUUM-3 obtained by reducing the source size by a factor of 15 to account for the possible increase in source size due to scattering, but does not fit the observations (see Gopalswamy and Kundu, 1990 for more details).

observed, the ending frequency is remarkably close to 8 MHz. The ending frequency translates to a maximum heliocentric distance for the radio source. Since the 8 MHz plasma level occurs around 3 $R_\odot$, the magnetic structures that support the type IV emission must extend to this height. It is not clear why the loops extend to large heights only after certain CMEs implied by the rarity of type IV bursts. It must be pointed out that Fig. 6 includes only the brightest of the type IV bursts. A systematic survey is needed to identify all the type IV bursts to obtain more accurate results.

4 Long wavelength Type III Radio Bursts

Type III bursts are one of the best indicators of release of electron beams near the Sun along open magnetic field lines. *In situ* observations of energetic electrons in association with these type III bursts have confirmed that a beam-plama instability involving the electron beams and the coronal plasma is ultimately responsible for the observed electromagnetic radiation. Extensive literature exists on the type III bursts (see, e.g. Dulk, 2000). In this paper, we concentrate on two variants: complex type III bursts and type III storms. Complex type III bursts were first identified in ISEE-3 radio data by Cane et al. (1981), who suggested that the responsible electrons were accelerated by flare blast waves. Type III storms are related to the metric noise storms, which are known to be caused by electrons accelerated in active regions by a non-eruptive process (Reiner et al. 2001a, and references therein).

4.1 Complex type III bursts: Source of Electrons

The source of nonthermal electrons for complex type III bursts has been debated extensively: flare blast waves (Cane et al. 1981), flares (Kundu and Stone, 1984; Klein, 1995; Bougeret et al.,

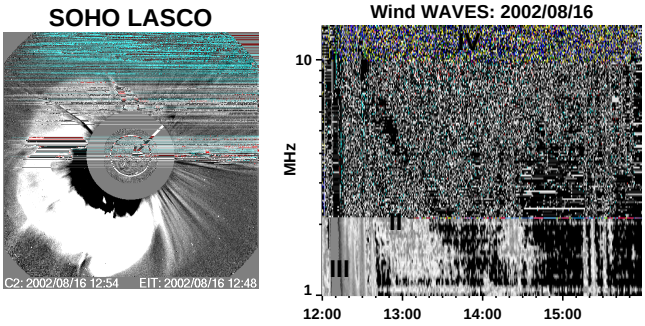

Figure 5: (right) Dynamic spectrum of the WAVES type IV burst of 2002 August 16. Preceding type II and type III bursts are marked. The irregular structure parallel to the marked type II burst may be the harmonic component of the type II. Note the U-shaped structure of the low-frequency end of the type IV burst. (left) SOHO's LASCO (12:54 UT) and EIT (12:48 UT) difference images showing the white-light CME and the source region (pointed by arrow), respectively. The dark feature in the LASCO image corresponds to the CME in the previous frame at 12:30 UT. In the image shown, the CME leading edge was already at a heliocentric distance of 6.7 $R_\odot$ at 12:54 UT. The CME originated from NOAA active region 0069 located at S14E20.

1998; Reiner et al., 2000; Cane et al., 2002) or CME-driven shocks (Gopalswamy et al., 2000; Klassen et al. 2002). Recent results indicate that there is a 100% association between large SEP events and complex type III bursts (MacDowall et al. 2003). Almost all large SEP events are also associated with fast and wide CMEs (Gopalswamy et al., 2003a), so it is natural to conclude that electrons, like ions, are also accelerated by CME-driven shocks. Simnett et al. (2002) concluded that relativistic electrons detected in space are accelerated in CME-driven shocks, but delayed by a few minutes with respect to the onset times of complex type III bursts. When CME-driven shocks can accelerate relativistic electrons, there is no reason why they cannot accelerate lower energy electrons (type III bursts need electrons with an energy of tens of keV). Although the presence of a CME is essential for the complex type III bursts, it is still not clear whether they are accelerated by the CME-driven shock or in the reconnection process taking place behind the CMEs. Since flares occupy a much smaller volume than CMEs, imaging these complex type III

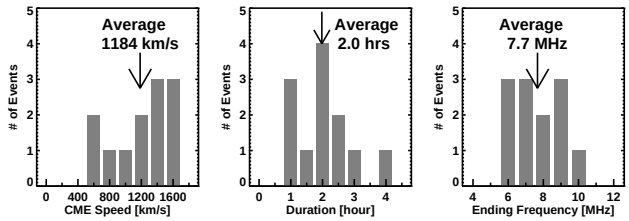

Figure 6: Statistical properties of the 12 WAVES type IV bursts observed between 1997 and 2002: (left) speed of the associated white-light CMEs, (middle) duration of type IV bursts at 14 MHz, and (right) ending frequency of the type IV bursts. The averages of the distributions are indicated. The upper part of the ending frequency is expected to merge with the metric type IV bursts.

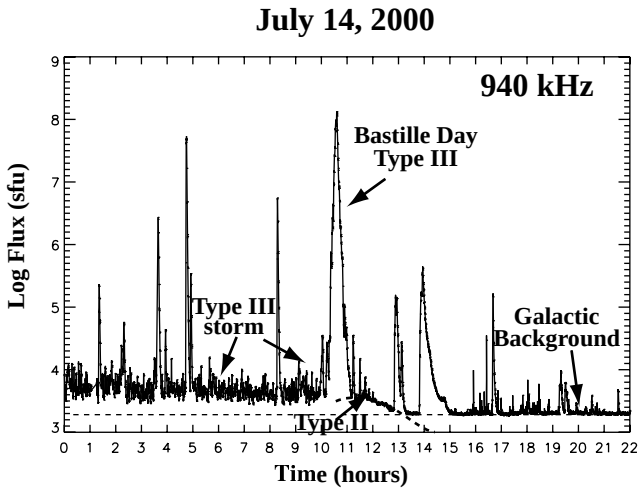

Figure 7: A single-frequency cut from the dynamic spectrum of the 2000 July 14 (Bastille day) event. The large bursts are the normal type III bursts. The "Bastille Day Type III" is a complex type III burst associated with a full halo CME. The short-duration fluctuations to the left of the Bastille Day type III constitute the type III storm. The type II burst associated with the CME is marked by the slanted dashed line. Note that the noise storm ceases at the time of the CME and the background emission lowers to the level of the galactic background (see Reiner et al., 2001a for more details).

bursts may be able to discriminate between these two possibilities based on the relative location and extent of the radio source.

4.2 Type III Storms

Type III storms are closely related to noise storms at metric wavelengths. Noise storms consist of short-duration bursts (known as type I bursts) superposed on a continuum emission. Noise storms occur above active regions, typically not associated with any eruption. As active regions evolve, small-scale energy release occurs quasicontinuously, which result in the observed radio emission. Some stationary type IV bursts are also known to evolve into noise storms. The weak noise storm shown in Fig. 2 occurred above two active regions, probably in the closed fields connecting the two regions (Kundu and Gopalswamy, 1990). Type III storms have been found to be the long-wavelength extensions of type I storms (Aubier et al. 1978). Space-based observations at kilometric wavelengths by the ISEE-3 spacecraft provided extensive information on the density and magnetic field structure of the inner heliosphere. Observations of a large number of kilometric type III storms indicated that the radio source regions extended to 100-170 $R_\odot$ from the Sun center (Bougeret et al., 1984a,b). The spacecraft observations also confirmed the type I - type III storm relationship suggesting that the electrons are accelerated low in the corona and propagate along density structures overlying active regions (Bougeret et al., 1984b). Thus the type III storm is essentially a long wavelength phenomenon, starting at decametric wavelengths and continuing into the kilometric domain. The storms are observed extensively by the WAVES experiment, providing a link between what was known before in the decametric and kilometric domains. Eruptions such as flares and CMEs also occur in active regions that

support noise storms. How the eruptions affect the noise storms depends on the nature of the eruption. Eruptive flares are known to switch off noise storms (Aurass et al., 1993). On the other hand, flares confined to the low-lying loops of the active region may not affect the noise storm located on the outermost structures of the active region (see, e.g. Gopalswamy et al., 1995). When a CME happens in an active region with an ongoing type III storm, the storm disappears temporarily or permanently. Chertok et al. (2001) reported sharp decreases of metric noise storms associated with CMEs. The decrease suggests a physical interaction between the CME and the magnetic structures carrying the noise storm. Since the type III storm is an extension of the metric noise storm, one would expect a similar disruption at longer wavelengths. This was in deed the case for the type III storm associated with NOAA AR 9077 (see Figure 7). The storm was present for a couple of days before the Bastille-day CME occurred on 2000 July 14 (Reiner et al., 2001a). The short-duration, low-intensity bursts that contituted the type III storm disappeared immediately after the CME eruption. The storm did not recover, which may indicate a permanent restructuring of the active region magnetic field. This provides an excellent opportunity to study the eruption and reformation of active region magnetic field structure.

5 Type II Bursts

Type II bursts (Wild and McCready, 1950) are confined to frequencies $\leq$ 150 MHz, although occasionally they are observed at higher frequencies (Vršnak et al., 1995). Metric type II bursts correspond to shocks in the inner corona, while DH and longer wavelength type II bursts are indicative of shocks propagating from the Sun far into the IP medium. Type II bursts were first observed in the IP medium by radio instruments on board the IMP-6 spacecraft (Malitson et a., 1973). Fast mode MHD shocks propagating through the corona and IP medium are thought to be responsible for the type II bursts. The shocks accelerate nonthermal electrons, which in turn produce radio emission at the fundamental and harmonic of the local plasma frequency via well known plasma processes. This scenario is confirmed by *in situ* observations of a shock, plasma waves and electrons (Bale et al., 1999) at the time of the type II burst.

The energy source of the shock has been controversial (see Gopalswamy et al., 1998; Cliver et al., 1999; Gopalswamy, 2000 for recent views). The two currently debated sources are flare blast waves and CME-driven shocks. The situation is complicated by the fact that most CMEs are also accompanied by flares. Positional information available for a limited number of type II bursts indicated that the radio sources occurred well behind the leading edge of the associated CMEs (Wagner and MacQueen, 1983; Gary et al., 1984; Robinson and Stewart, 1985; Gopalswamy and Kundu, 1992b). Flare shocks moving through the associated CME material may produce such a source position, provided the CME-driven shock does not produce type II bursts (Wagner and MacQueen, 1983). An alternative would be radio emission produced only at the flanks of the CME-driven shock. In sky-plane projection, the flanks and hence the radio sources would appear below the leading edge for limb CMEs. This scenario is consistent with the idea that quasi-perpendicularity (required for electron acceleration) prevails at the flanks of the CME-driven shock (Holman and Pesses, 1983). Cane (1983) found a mismatch between the drift rates of type II bursts above and below 1 MHz. This was considered to be evidence for the existence of two types of shocks discussed above. However, if the high frequency radio emission originates from the flanks and the low frequency emission comes from the nose of the same shock, one would expect a mismatch between the drift rates because the flanks and nose travel at different

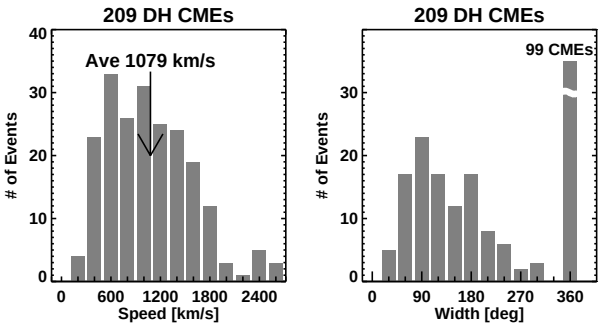

Figure 8: The speed and width distributions of CMEs associated with the DH type II bursts (and hence these CMEs are labeled as DH CMEs) for the period 1997-2002. There were actually 350 bursts, but excluding those that occurred during SOHO data gaps and the purely kilometric type II bursts, we ended up with 209 events, which we included in the statistics. Note that nearly half of the CMEs were halo events and the rest are much wider than normal CMEs. In the 360° bin, the bar is shown broken to note that the large number (99) of CMEs. The average speed of the DH CMEs is indicated by an arrow.

speeds. This may also be the reason for the poor correlation between CME speeds measured in the outer corona and the shock speeds derived from the metric type II bursts (Reiner et al., 2001b). Recent observations have shown that successive fast CMEs can originate from the same active region (Gopalswamy et al., 2003c). This raises the possibility that two successive CMEs may mimic the two-shock situation (CME-driven shock followed by blast wave from the same eruption).

Although the blast wave origin for metric type II bursts is consistent with the observation that a third of the metric type II bursts were not associated with white light CMEs (Sheeley et al. 1984), Cliver et al. (1999) pointed out that this lack of association can be attributed to the visibility problem: the type II bursts lacking CME association originated predominantly from the solar disk. Coronagraphs which detect CMEs have the inherent difficulty of not being able to efficiently detect disk CMEs. Gopalswamy et al. (2001a) also found the lack of CME association for ∼34% of metric type II bursts, but all of were disk events that had clear EUV transients. This confirms the conclusions of Cliver et al. (1999) that type II bursts are essentially a CME-related phenomenon.

All kilometric type II bursts observed by ISEE-3 are known to be associated with CMEs and IP shocks (Cane et al., 1987). Recent data from Wind/WAVES indicate that all DH type II bursts are also associated with fast and wide CMEs capable of driving shocks (Gopalswamy et al., 2001b). Figure 8 shows the speed and width distributions of CMEs associated with DH type II bursts for the period 1997-2002. Can we extend this CME-type II connection to metric type II bursts also? Lara et al. (2003) studied the CME properties of metric type II bursts with no IP counterparts and compared them with those of DH type II bursts. They found that the speed, width and deceleration of CMEs progressively increased for the general population of CMEs, CMEs associated with metric type II bursts and CMEs associated with IP type II bursts, in that order. This is a clear evidence that the energy of a CME is an important factor in deciding whether it will be associated with a type II burst. This, of, course is not the whole story. Gopalswamy et al. (2001b) has found that 60% of the fast CMEs (speed > 900 km s^{-1}) did not have DH type II bursts. Even after eliminating fast CMEs with width $< 60°$, there

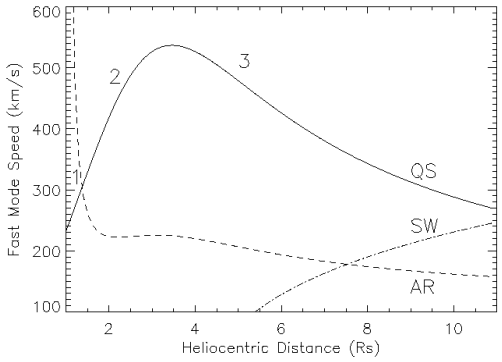

Figure 9: Radial profile of the fast-mode speeds in the quiet (solid curve, marked QS) and in the active region (dashed line, marked AR) coronas. Region 1 represents the region of high fast-mode speed in the active region, where it is difficult to form shocks. Region 2 corresponds to the metric domain, where it is relatively easy to form shocks. Region 3 corresponds to the IP medium, where the fast-mode speed declines. Solar wind speed (radial profile denoted by SW) picks up from a few solar radii and becomes significant beyond about 8 solar radii (see Gopalswamy et al., 2001a for details).

remained a significant fraction of fast and wide radio-quiet CMEs. To explain this one has to recall that the ability of a CME to drive a shock depends not only on its speed, but also on the properties of the medium through which the CME propagates.

R M Infiles s c ri t rio fo shoc for atio i tha th CM spee relativ t the ambie x ee th fas mod spee (fod

A the regio of r u Gopalswamm 20

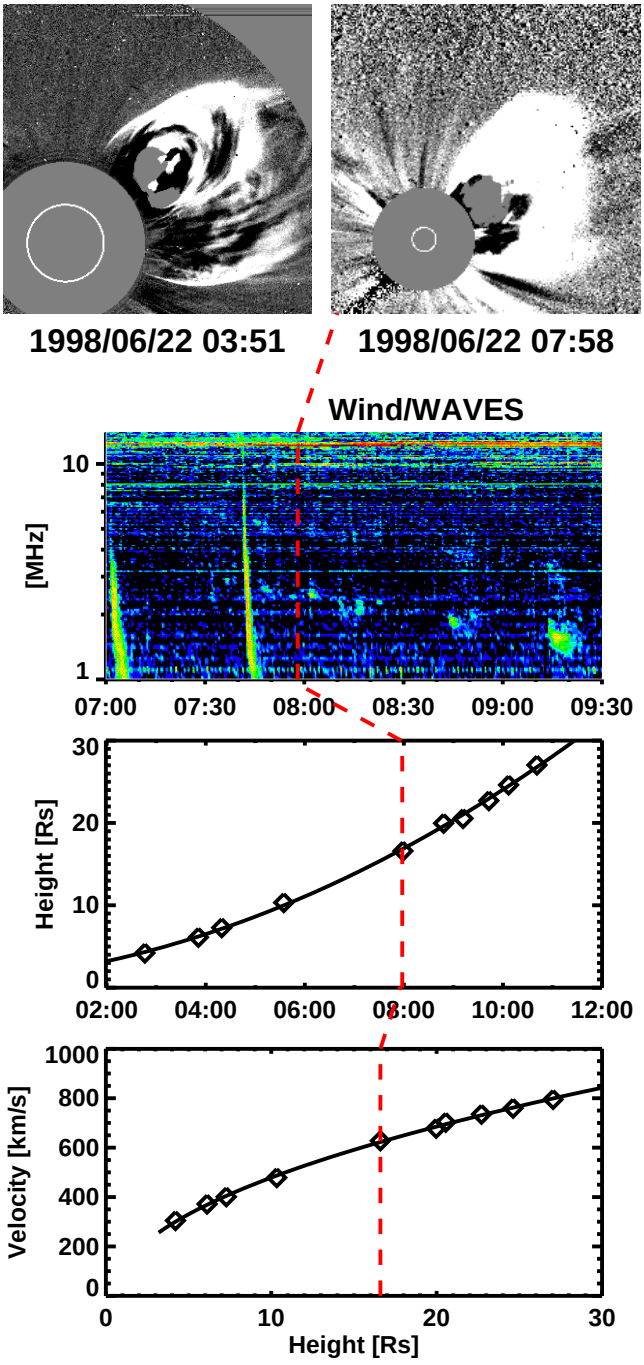

Figure 10: SOHO/LASCO difference images showing the 1998 June 21-22 CME (top panel), the associated type II radio emission observed by Wind/WAVES (intermittent slanted features in the upper middle panel), CME height-time plot from 02:00 to 12:00 UT on 1998 June 22 (lower middle panel), and the evolution of CME speed with heliocentric distance in units of solar radii, R_s (bottom panel). The instance of the second LASCO image is marked on all the plots by the vertical dashed line.

5.1 Type II burst associated with a slowly-accelerating CME

A slowly-accelerating CME on 1998 June 21 was associated with a weak type II burst in the IP medium. Figure 10 summarizes the event with snap-shot images of the CME at two instances, the WAVES dynamic spectrum, the CME height-time plot and the evolution of CME speed with height. The radio emission in question started at $\sim$ 5 MHz and was weak and intermittent, but had fundamental-harmonic structure. The radio emission started around 08:00 UT on June 22 and lasted for 1.5 h. The CME first appeared in the LASCO field of view at 18:15 UT on 1998 June 21. Extrapolation of the height-time plot to the surface gives an onset time of 14:59 UT on June 21. The average acceleration was only 1.4 m s^{-2} but persisted all the way to the edge of the LASCO field of view. Srivastava et al., (2000) tracked the changes in the acceleration and found that it peaked when the CME was at a distance of 4 $R_\odot$, but remained positive until the CME reached a distance of 20 $R_\odot$. The CME attained a speed of 400 km s^{-1} only when it reached a height of 6 $R_\odot$. When the radio emission started, the CME was already at a distance of 16.5 $R_\odot$ moving with a speed of $\sim$600 km s^{-1}. The interpretation is that the CME attains super-Alfvenic speed only at a large distance from the Sun and starts driving a shock resulting in the production of the type II burst. This CME illustrates the importance of CME speed for its association with a type II burst. At large distances from the Sun, the solar wind speed becomes important, so the CME speed relative to the solar wind speed has to exceed the local Alfven speed to drive a fast mode shock.

5.2 Some statistics on Type II bursts

The basic picture of CME-type II association described above is also reflected in statistical analyses. Nearly 7000 CMEs were detected by SOHO between 1996 and 2002. Over the same period, there were only 736 metric type II bursts, suggesting that only $\sim$10% of CMEs are associated with metric type II bursts. The total number of IP type II bursts (f $<$ 14 MHz) is only 350. Therefore, type II bursts are a relatively rare phenomenon. Interestingly, the number of fast (speed $>$ 900 km s^{-1}) CMEs is also similar (450). Figure 11 compares the number of metric and DH type II bursts with the rate of white-light CMEs averaged over Carrington Rotations. The number of DH type II bursts is generally smaller than that of the metric type II bursts. The metric type II bursts have a better correlation with the CME rate than the DH type II bursts. This is because, the DH type II bursts are associated with faster and wider CMEs. It was shown by Gopalswamy et al. (2003b) that the peaks in DH type II rate coincided with the peaks in the mean speed of CMEs.

DH type II bursts indicate the presence of fast and wide CMEs driving shocks. Most of the large SEP events are also associated with DH type II bursts (Gopalswamy, 2003). From these results we can infer that the same shocks accelerate both electrons and ions. To illustrate this we have compared the rates of DH type II bursts, major SEPs, and IP shocks in Fig. 12. First of all we note that the numbers are comparable. The small differences are expected because the observability differs from one another. For example, SEPs are better observed when they are well connected to the observer. DH type II bursts can be observed from limb CMEs without any problem, but only a flank of the shocks is expected at 1 AU. It is also possible that some flanks become too weak to remain as shocks by the time they get to 1 AU. Allowing for these caveats, we can conclude that DH type II bursts can clearly isolate the small number of SEP-effective CMEs. Imaging the long wavelength type II bursts at multiple frequencies can actually provide the direction and speed of the shock when it is still close to the Sun, which are crucial for space

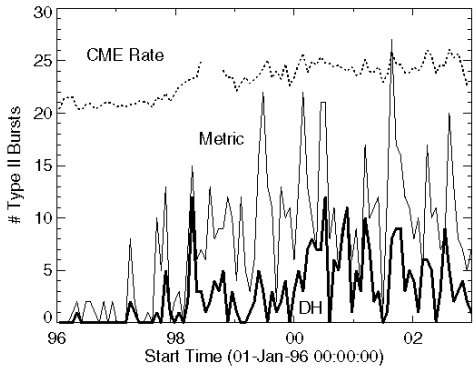

Figure 11: Relative occurrence of metric (thin lines) and DH (thick lines) type II bursts summed over Carrington Rotation periods. The CME rate (dotted lines) from Gopalswamy et al. (2003a) is also shown for comparison. Daily CME rate was obtained by averaging over CR. To the actual CME rate we have added 20 to fit the plot within the scale. The break in the CME rate curve is due to the major data gap during June - October 1998 when SOHO was temporarily disabled.

weather predictions.

6 Radio Signatures of CME Interaction

CME interactions were first identified as long wavelength radio enhancements in the Wind/WAVES dynamic spectra (Gopalswamy et al., 2001c; 2002a). The typical radio signature of CME interaction could be described as the modification of the dynamic spectrum of a normal type II burst. This modification stems from the basic requirement that the CME must drive a fast mode shock, which happens when the CME moves with a super-Alfvenic speed. When a density (n) or magnetic field (B) inhomogeneity is present in the ambient medium through which the CME-driven shocks propagate, the upstream Alfven speed (Va) will be modified according to the relation, $dVa/Va = dB/B$ - (1/2) dn/n. The simplest interpretation for the radio enhancement is that the increased density in the upstream medium lowers the upstream Va thereby increasing the Mach number of the shock. Numerical simulations have confirmed such shock strengthening (Wu et al., 2002; Odstrčil et al., 2003). Although interactions among shocks and ejecta have been known for a long time from *in situ* observations (Burlaga et al., 1987), those occurring very close to the Sun are particularly important because the CME-driven shocks are most potent there. In addition to the strength of the magnetic field, its topology can also affect particle acceleration: trapping of particles in the closed loops of preceding CMEs can repeatedly return the particles back to the shock, thus enhancing the efficiency of acceleration (Gopalswamy et al., 2002b; Kallenrode and Cliver 2001). Radio signatures have been observed from interacting CMEs originating in the same solar source or from neighboring regions (Gopalswamy et al., 2003a). Systematic survey is needed to classify the radio signatures so that the underlying mechanism of interaction can be better understood. In this section, we describe two cases in which the interacting CMEs occurred in quick succession.

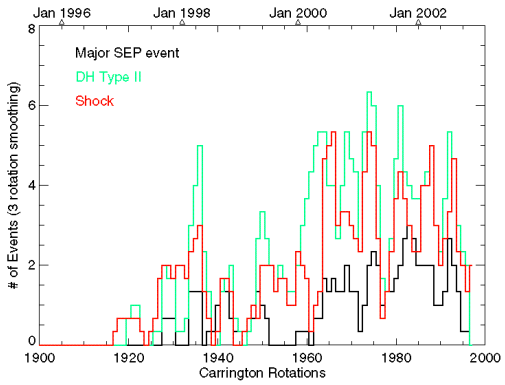

Figure 12: Comparison between DH type II bursts, SEPs and IP shocks as a function of time (as Carrington Rotation numbers at the bottom and universal time at the top) . The numbers are smoothed over three Carrington rotations. The major SEP events are defined as those with GOES proton intensity in the $>$ 10 MeV channel exceeding 10 particles per (cm^2 s sr). The IP shocks were detected in *in situ*. The DH type II bursts were observed by the Wind/WAVES experiment.

6.1 Radio Signatures of Closely Spaced CMEs: Case Study 1

The asymmetric halo CME of 2001 December 25 originated from above the southeast limb and had an average speed of 1773 km s^{-1}. This CME was associated with a broadband (10 MHz) radio enhancement lasting for about 45 min (see the WAVES dynamic spectrum in Fig. 13). The CME was preceded by a slow draining of a large-scale bright streamer. In addition, the helmet of the streamer was expanding slowly with a speed of $\sim$ 87 km s^{-1}. This structure can be seen as the outermost dark void in the 10:57 UT LASCO image shown in Fig. 13. A narrow CME with an onset time of 09:30 UT appeared behind the helmet and was seen above the LASCO/C2 occulting disk at 10:34 UT. This CME can also be seen in the 10:57 UT frame in Fig. 13 as the brightest feature protruding above the limb and was moving with a speed of 245 km s^{-1} at a position angle of 134°. This CME was seen distinctly in the 11:07 UT frame (not shown). In the 11:30 UT frame, the fast CME appeared within the C2 field of view at a heliocentric distance of 5.56 R$_\odot$. The height-time plot extrapolated to the surface gives an onset time of 10:59 UT. The height-time plots of all the three CMEs are shown in Fig. 13. The insufficient cadence of LASCO images does not permit us to get the exact time of interaction, but it is clear that the radio enhancement started around the time of the intersection of trajectories (before the time of first appearance of the halo CME). The interaction signature ended by 12:00 UT, when the CME was at a height of 10 R$_\odot$. At the same time a narrow band type II burst continued to lower frequencies with no interaction signature. This suggests that the CME and its associated shock have moved past the spatial region occupied by the two preceding CMEs. This case is different from the 2000 June 10 event (in which the interaction signature was first detected) in that the normal type II burst followed the interaction signature. A closer look at the interaction signature reveals that it also has fundamental-harmonic structure. The fundamental emission

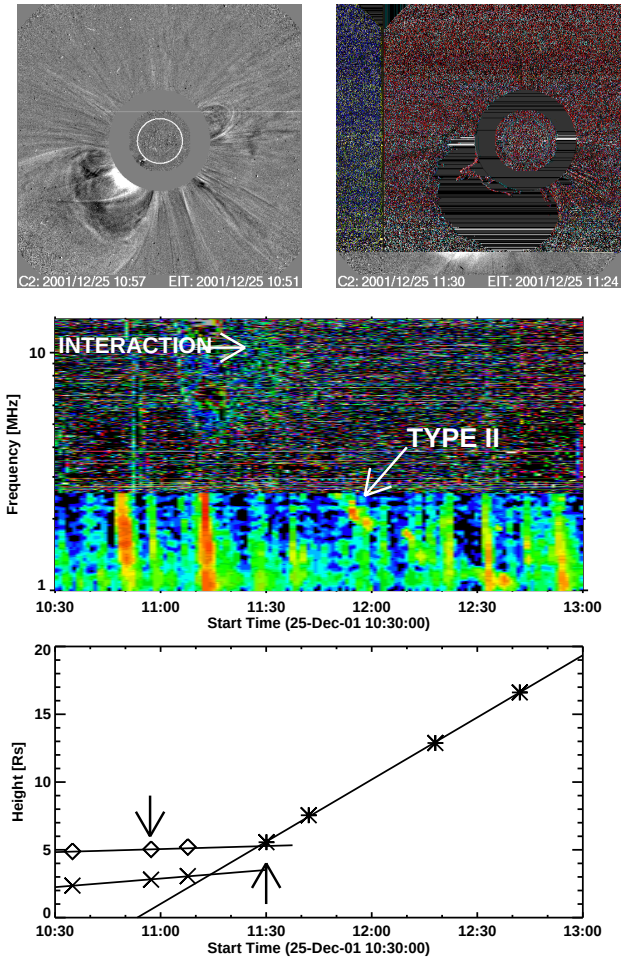

Figure 13: LASCO and Wind/WAVES observations of the 2001 December 25 interaction event. (top left) LASCO difference images at 10:57 UT showing the void and a preceding slow CME. (top right) LASCO difference image showing the fast CME at 11:30 UT. (middle) Wind/WAVES dynamic spectrum showing the broadband interaction signature and a normal type II burst associated with the fast CME. (bottom) height-time plots of the helmet streamer (diamonds), the slow CME (crosses) and the fast CME (asterisks). Height-time measurements corresponding to the displayed LASCO frames are pointed to by vertical arrows in the bottom panel.

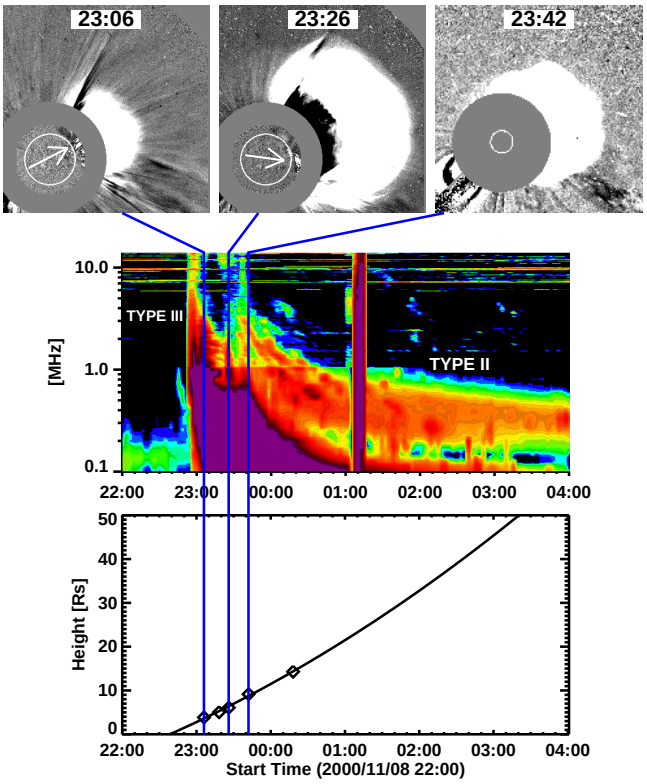

Figure 14: Snapshots of the SOHO/LASCO CME (top), WAVES dynamic spectrum (middle) and CME height-time plot of the CME (bottom) for the 2000 November 08 data. EIT difference images are superposed on the 23:06 and 23:26 UT LASCO images and the eruption regions are marked by arrows. Times of the selected LASCO frames are marked by the vertical lines on the two bottom panels. In the dynamic spectrum, the type III and Type II bursts are marked. The height-time plot is extrapolated to show that the radio emission remained strong even beyond 50 $R_{\odot}$.

starts at 8 MHz. The harmonic structure should have started at 16 MHz, which is outside the WAVES spectral range. The WAVES dynamic spectrum shows that the harmonic structure must have started above its highest frequency (14 MHz). Although no metric type II burst was reported in the Solar Geophysical Data, Potsdam observatory reported a type II starting at 70 MHz around 11:16 UT and drifting to 40 MHz within 1.3 min. There is clearly a gap between the metric and DH radio emission, but the differences can be explained by the shock geometry as discussed in section 5.

6.2 Radio Signatures of Closely Spaced CMEs: Case Study 2

Figure 14 shows the 2000 November 8 event consisting of an intense type II burst at frequencies less than 5 MHz and halo CME. The WAVES dynamic spectrum had two distinct episodes of radio emission: a complex type III burst during 22:54 to 23:08 corresponding to metric type III bursts reported from Culgoora (SGD, 2000 November 8). After a gap of about 10 min, the radio emission again started at 23:18 as a diffuse vertical structure. The IP type II burst appeared as

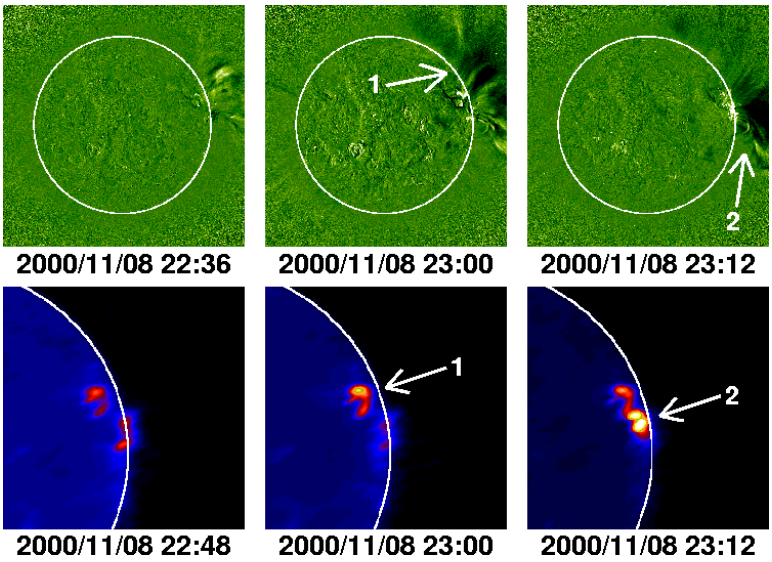

Figure 15: EIT difference images (top) and Nobeyama radioheliograph images at 17 GHz (bottom) showing the solar sources of the two eruptions (marked 1 and 2) on 2000 November 8. In the 17 GHz images, only the northwest quadrant of the Sun is shown.

a continuation of this episode. Even though no metric type II burst was reported, the dynamic spectrum from the Hiraiso radio spectrograph indicated a brief episode of type II burst around 23:15 UT (Gopalswamy, 2003). When the associated CME first appeared in the LASCO/C2 field of view 23:06, it was already at a height of 3.85 $R_\odot$. Linear fit to the height-time plot gives a speed of 1738 km s^{-1}. The EIT images showed two eruptions, one at 22:36 UT slightly above the equator causing a large depletion above the limb at 23:00 UT and the other at 23:12 slightly to the south (see Fig. 15). The microwave images from the Nobeyama radioheliograph also confirmed the two neighboring eruptions. The two eruptions came from the AR complex consisting of ARs 9222, 9218, 9212, and 9213. Three SOHO/LASCO difference images are shown in Fig. 14 with the EIT difference images superposed to show the EUV eruptions. It appears that the 23:06 UT frame contains the first CME while the frame at 23:26 UT contains a compound of two CMEs. The sudden and unusually high acceleration (70 m s^{-2}) at the time of the second eruption is also suggestive of the two closely-spaced eruptions. The CME height-time plot is extrapolated to show that the IP type II burst remained intense far beyond 50 $R_\odot$. If we exclude the data point at 23:06 UT, the CME height-time plot will not show such extreme acceleration. The snapshot images in Fig. 14 also show that the CME at 23:06 is heading northwest radially above the first EUV eruption. At 23:26 UT, the CME has more extension to the southwest, directly above the second EUV eruption. Thus by 23:26, we believe that the two CMEs merged to produce a compound CME driving the shock responsible for the IP type II burst. The shock arrived at Earth at 06:15 UT on November 10, in about 30 h as detected by the WAVES Thermal Noise Receiver (not shown). Whenever such closely spaced

eruptions occur, the type II burst associated with the second CME is strong and long-lasting (Gopalswamy et al., 2003a).

7 Concluding Remarks

We highlighted several issues related to the thermal and nonthermal radio emission from the Sun at long wavelengths. In addition to reviewing past observations, we described new results based on observations from the Wind/WAVES experiment with complementary information from the SOHO mission. Notably, we described type IV bursts in the decametric domain, radio signatures of colliding CMEs, and the solar-cycle variation of particle-accelerating shocks. Even though Wind/WAVES experiment has little spatial information of the bursts, its high-frequency (1-14 MHz) receiver probes plasma levels within the field of view of the SOHO coronagraph. This has helped us understand the relation between shocks (inferred from radio observations) and their CME drivers (detected in white light). The coronagraphic data contain information on the density of the ambient medium, which is an important factor deciding shock formation and propagation of shocks in addition to the CME kinetic energy. The role played by the ambient conditions in deciding the formation and propagation of shocks is evident from the behavior of the radial profile of the fast-mode speed in the corona. Variation of the Alfven speed profile with latitude and longitude, and due to transient conditions such as interacting CMEs needs to be quantified to fully understand the complex relationship between CMEs and shock-related radio bursts. Interestingly, all the other burst types discussed in this paper are in someway related to CMEs: complex type III bursts, type III storms, and type IV bursts. Further exploration of this relationship is likely to yield more information on the evolution of CMEs and their interaction with other structures.

One of the interesting outcomes of the combined study of the radio bursts and white light CMEs is the possibility to isolate the tiny fraction of all CMEs that directly affect Earth's space environment. These CMEs are responsible for driving shocks in the near-Sun IP medium, which seem to accelerate electrons (as inferred from IP type II bursts) and protons (detected *in situ*). Solar cycle variation of these large scale CMEs is more pronounced compared to the ordinary CMEs and the close correlation of CMEs, shocks and type II radio bursts establishes the physical relationship among these phenomena. The logical next step would be to image the radio bursts so that the physical relationship between CMEs and type II bursts can be directly confirmed beyond the temporal association available at present. Imaging at frequencies in the range 1-30 MHz is ideal for getting information on solar eruptions in the near-Sun interplanetary medium. A combination of ground based imaging by the Low Frequency Array (LOFAR) and space based imaging by the Solar Imaging Radio Array (SIRA) would be ideal to make rapid progress on eruptions that may have significant influence on the inner heliosphere.

Acknowledgments: I thank M. L. Kaiser for Wind/WAVES data, S. Yashiro and A. Lara for help with figures, and E. Aguilar for help with the manuscript. SOHO is a project of international cooperation between NASA and ESA. This research was supported by NASA/LWS and NSF/SHINE (ATM 0204588) programs.

References

Aubier, M. G., Leblanc, Y. & Moller-Pederson, B., 1978. Type I and Type III Storm Radiation. Astron. Astrophys. 70, 685-693.

Aurass, H., Hofmann, A., Magun, A., Soru-Escaut, I., & Zlobec, P., 1993. Evaporation causes flare-related radio burst continuum depressions, Solar Phys., 145, 151-168.

Bale, S. D., Reiner, M. J., Bougeret, J.-L., Kaiser, M. L., Krucker, S., Larson, D. E., Lin, R. P., 1999. The source region of an interplanetary type II radio burst. Geophys. Res. Lett. 26, 1573-1576.

Bastian, T. S., Pick, M., Kerdraon, A., Maia, D., Vourlidas, A., 2001. The Coronal Mass Ejection of 1998 April 20: Direct Imaging at Radio Wavelengths. Astrophys. J. 558, L65-L69.

Bougeret, J.-L., Fainberg, J., & Stone, R. G., 1984a. Interplanetary radio storms. I - Extension of solar active regions through the interplanetary medium. Astron. Astrophys. 136, 255-262.

Bougeret, J.-L., Fainberg, J., & Stone, R. G., 1984b. Interplanetary radio storms. II - Emission levels and solar wind speed in the range 0.05-0.8 AU, Astron. Astrophys. 141, 17-24.

Bougeret, J.-L. et al., 1995. Waves: The Radio and Plasma Wave Investigation on the Wind Spacecraft. Space Sci. Rev. 71, 231-263.

Bougeret, J.-L. et al., 1998. A shock-associated (SA) radio event and related phenomena observed from the base of the solar corona to 1 AU. Geophys. Res. Lett. 25, 2513-2516.

Burlaga, L. F., Behannon, K. W., & Klein, L. W., 1987. Compound streams, magnetic clouds, and major geomagnetic storms. J. Geophys. Res., 92, 5725 -5734.

Cane, H. V. 1983. Velocity profiles of interplanetary shocks. NASA Conf. Publ., CP-2280, 703-709.

Cane, H. V., Stone, R. G., Fainberg, J., Steinberg, J. L., Hoang, S., Stewart, R. T., 1981. Radio evidence for shock acceleration of electrons in the solar corona. Geophys. Res. Lett. 8, 1285-1288.

Cane, H. V. et al., 1987. Energetic interplanetary shocks, radio emission, and coronal mass ejections. J. Geophys. Res., 92, 9869-9874.

Cane, H. V., Erickson, W. C. & Prestage, N. P., 2002. Solar flares, type III radio bursts, coronal mass ejections, and energetic particles. J. Geophys. Res. 107, issue 10, SSH 14-1.

Cliver, E. W., Webb, D. F., & Howard, R. A., 1999. On the origin of solar metric type II bursts. Solar Phys., 187, 89-114.

Dulk, G. A., 2000. Type II Solar Radio Bursts at Long Wavelengths. Radio Astronomy at Long Wavelengths, Geophysical Monograph 119, AGU, Washington DC, 115-122.

Gary, D. E., et al., 1984. Type II bursts, shock waves, and coronal transients - The event of 1980 June 29, 0233 UT. Astron. Astrophys. 134, 222-233.

Gopalswamy, N., 2000. Type II Solar Radio Bursts. Radio Astronomy at Long Wavelengths,

Geophysical Monograph 119, AGU, Washington DC, 123-135.

Gopalswamy, N., 2003. Solar and geospace connections of energetic particle events. Geophys. Res. Lett. 30, 1-4.

Gopalswamy, N., Raulin, J.-P., Kundu, M. R., Nitta, N., Lemen, J. R., Herrmann, R., Zarro, D., Kosugi, T., 1995. VLA and YOHKOH Observations of an M1.5 Flare. Astrophys. J. 455, 715-732.

Gopalswamy, N. & Kundu, M. R., 1990. Multiple moving magnetic structures in the solar corona. Solar Phys. 128, 377-397

Gopalswamy, N. & Kundu, M. R., 1992a. Estimation of the mass of a coronal mass ejection from radio observations. Astrophys. J. 390, L37-L39.

Gopalswamy, N. & Kundu, M. R., 1992b. Are coronal type II shocks piston driven? AIP Conference Proceedings # 264: Particle Acceleration in Cosmic Plasmas, ed. by G. P. Zank & T. K. Gaisser, American Institute of Physics, New York, 257-260.

Gopalswamy, N. et al., 1998. Origin of coronal and interplanetary shocks - A new look with WIND spacecraft data. J. Geophys. Res., 307-316.

Gopalswamy, N. & Kundu, M. R.1993. Thermal and nonthermal emissions during a coronal mass ejection. Solar phys., 143, 327-343.

Gopalswamy, N. et al., 2000. Radio-rich Solar Eruptive Events. Geophys. Res. Lett., 27, 1435-1439.

Gopalswamy, N., Lara, A., Kaiser, M. L., Bougeret, J.-L., 2001a. Near-Sun and near-Earth manifestations of solar eruptions. J. Geophys. Res. 106, 25261-25278.

Gopalswamy, N., Yashiro, S., Kaiser, M. L., Howard, R. A., Bougeret, J.-L., 2001b. Characteristics of coronal mass ejections associated with long-wavelength type II radio bursts. J. Geophys. Res. 106, 29219-29230.

Gopalswamy, N., Yashiro, S., Kaiser, M. L., Howard, R. A., Bougeret, J.-L., 2001c. Radio Signatures of Coronal Mass Ejection Interaction: Coronal Mass Ejection Cannibalism? Astrophys. J. 548, L91-L94.

Gopalswamy, N. & Kaiser, M. L., 2002. Solar eruptions and long wavelength radio bursts: The 1997 May 12 event. Adv. Space Res., 29(3), 307-312.

Gopalswamy, N., Yashiro, S., Kaiser, M. L., Howard, R. A., & Bougeret, J.-L., 2002a. Interplanetary radio emission due to interaction between two coronal mass ejections. Geophys. Res. Lett., 29, 106-1.

Gopalswamy, N., Yashiro, S., Michałek, G., Kaiser, M. L., Howard, R. A., Reames, D. V., Leske, R., & von Rosenvinge, T., 2002b. Interacting Coronal Mass Ejections and Solar Energetic Particles. Astrophys. J., 572, L103-L107.

Gopalswamy, N., Yashiro, S., Lara, A., Kaiser, M. L., Thompson, B. J., Gallagher, P. T., Howard, R. A., 2003a. Large solar energetic particle events of cycle 23: A global view. Geophys. Res. Lett. 30, SEP 3-1.

Gopalswamy, N., Nunes, S., Yashiro, S. & Howard, R. A., 2003b. Variability of Solar Eruptions during cycle 23. Adv. Space Res., in press.

Gopalswamy, N., Yashiro, S., Stenborg, G., & Howard, R., 2003c. Coronal and Interplanetary Environment of Large Solar Energetic Particle Events, Proceeding of 28th International Cosmic Ray Conference. 3549.

Holman, G. D. & Pesses, M. E., 1983. Solar type II radio emission and the shock drift acceleration of electrons. Astrophys. J. 267, 837-843.

Kallenrode, M.-B., & Cliver, E. W., 2001. Rogue SEP events: Modeling. Proc. ICRC 2001, 3319-3321.

Kathiravan, C., Ramesh, R., & Subramanian, K. R., 2002. Metric Radio Observations and Ray-tracing Analysis of the Onset Phase of a Solar Eruptive Event. Astrophys. J. 567, L93-95.

Kerdraon, A., & Delouis, J. -M., 1997. The Nançay Radioheliograph. Coronal Physics from Radio and Space Observations, ed. G.Trottet (Lecture Notes in Physics 483; Berlin: Springer), 192.

Klassen, A., Bothmer, V., Mann, G., Reiner, M. J., Krucker, S., Vourlidas, A., & Kunow, H., 2002. Astron. Astrophys., 385, 1078-1088.

Klein, K.-L., 1995. Coronal Magnetic Energy Releases, Lecture Notes in Physics, 444, 55.

Krogulec, M., Musielak, Z. E., Suess, S. T., Nerney, S. F., & Moore, R. L., 1994. Reflection of Alfven waves in the solar wind. J. Geophys. Res. 99, 23489-23501.

Kundu, M.R., 1965. Solar Radio Astronomy, Interscience Publishers, New York.

Kundu, M. R., Erickson, W. C., Gergely, T. E., Mahoney, M. J., & Turner, P. J., 1983. First results from the Clark Lake Multifrequency Radioheliograph. Solar Phys. 83, 385-389.

Kundu, M. R., Gopalswamy, N., 1990. Filament eruption and storm radiation at meter-decameter wavelengths. Solar Phys. 129, 133-152.

Kundu, M. R. & Stone, R. G., 1984. Observations of solar radio bursts from meter to kilometer wavelengths. Adv. Space res., 4(7), 261-270.

Lara, A., Gopalswamy, N., Nunes, S., Muñoz, G., & Yashiro, S., 2003. A statistical study of CMEs associated with metric type II bursts. Geophys. Res. Lett. 30, No.12, SEP 4-1.

MacDowall, R. J., Lara, A., Manoharan, P. K., Nitta, N. V., Rosas, A. M., Bougeret, J. L., 2003. Long-duration hectometric type III radio bursts and their association with solar energetic particle (SEP) events. Geophys Res. Lett. 30, No. 12, SEP 6-1.

Maia, D., Pick, M., Vourlidas, A., & Howard, R., 2000. Development of Coronal Mass Ejections: Radio Shock Signatures. Astrophys. J. 528, L49-L51.

Malitson, H. H., Fainberg, J., & Stone, R. G., 1973. Observation of a Type II Solar Radio Burst to 37 R_{sun}. Astrophys. Lett. 14, 111.

Mann, G., Klassen, A., Estel, C., & Thompson, B. J., 1999. Coronal Transient Waves and

Coronal Shock Waves. Proc. of 8th SOHO Workshop, Edited by J.-C. Vial & B. Kaldeich-Schmann. 477-481.

Mann, G., Klassen, A., Aurass, H., Classen, H.-T., 2003. Formation and development of shock waves in the solar corona and the near-Sun interplanetary space. Astron. Astrophys. 400, 329-336.

Marqué, Ch., Lantos, P., Delaboudiniére, J. P., 2002. Multi wavelength investigation of the eruption of a sigmoidal quiescent filament. Astron. Astrophys. 387, 317-325.

McLean, D. J., Labrum, N. R., 1985. Solar radiophysics: Studies of emission from the sun at metre wavelengths. Cambridge University Press.

Odstrčil, D., Vandas, M., Pizzo, V., & MacNeice, P., 2003. Numerical simulation of interacting flux ropes. Solar Wind 10, AIP Conference Proceedings, Volume 679, pp. 699-702.

Ramesh, R., Subramanian, K. R., Sundararajan, M. S., & Sastry, C. V., 1998. The Gauribidanur Radioheliograph. Solar phys. 181, 439-453.

Ramesh, R., Kathiravan, C., & Sastry, C. V., 2003. Metric Radio Observations of the Evolution of a "Halo" Coronal Mass Ejection Close to the Sun. Astrophys. J., 591, L163-L166.

Reiner, M. J., Kaiser, M. L., Karlický, M., Jiřička, K., Bougeret, J.-L., 2001a. Bastille Day Event: A Radio Perspective. Solar Phys. 204, 121-137.

Reiner, M. J., Kaiser, M. L., Gopalswamy, N., Aurass, H., Mann, G., Vourlidas, A., Maksimovic, M., 2001b. Statistical analysis of coronal shock dynamics implied by radio and white-light observations. J. Geophys Res. 106, 25279-25290.

Robinson, R. D., 1985, Flare continuum. Solar radiophysics: Studies of emission from the sun at metre wavelengths, Cambridge and New York, p. 385-414.

Robinson, R. D. & Stewart, R. T., 1985. A positional comparison between coronal mass ejection events and solar type II bursts. Solar Phys., 97, 145-157.

Sheeley, N. R., Howard, R. A., Michels, D. J., Robinson, R. D., Koomen, M. J., & Stewart, R. T.1984. Associations between coronal mass ejections and metric type II bursts. Astrophys. J., 279, 839-847.

Sheridan, K. V., Jackson, B. V., McLear, D. J., & Dulk, G. A., 1978. Radio observations of a massive, slow moving ejection of coronal material. Proc. ASA, 3, 249-250.

Simnett, G. M., Roelof, E. C., & Haggerty, D. K., 2002. The Acceleration and Release of Near-relativistic Electrons by Coronal Mass Ejections. Astrophys. J. 579, 854-862.

Srivastava, N., Schwenn, R., Inhester, B., Martin, S. F., & Hanaoka, Y., 2000. Factors Related to the Origin of a Gradual Coronal Mass Ejection Associated with an Eruptive Prominence on 1998 June 21-22. Astrophys. J. 534, 468-481.

Stewart, R. T., 1985. Moving Type IV bursts. Solar radiophysics: Studies of emission from the sun at metre wavelengths, Cambridge and New York, p. 361-383.

Vršnak, B., Ružđjak, V., Zlobec, P., Aurass, H., 1995. Ignition of MHD shocks associated with

solar flares. Solar Phys. 158, 331-351.

Wagner, W. J. & MacQueen, R. M., 1983. The excitation of type II radio bursts in the corona. Astron. Astrophys., 120, 136-138.

Wild, J. P. & McCready, L. L., 1950. Observations of the spectrum of high-intensity solar radiation at metre wavelengths. I. The Apparatus and Spectral Types of Solar Burst Observed. Aust. J. Sci. Res., A3, 387-398.

Wu, S. T., Wang, A. H., & Gopalswamy, N., 2002. MHD modelling of CME and CME interactions in a bi-modal solar wind: a preliminary analysis of the 20 January 2001 two CMEs interaction event. SOLMAG 2002, Ed. H. Sawaya-Lacoste, ESA SP-505. Noordwijk, Netherlands, 227 - 230.

Zheleznyakov, V. V., 1969. Radio emission of the Sun and Planets. Pergamon Press, New York.